Bull. Chem. Soc. Jpn., 70, 2647—2655 (1997)

Crystal Structure and Physical Properties of (BEDT-TTF)$_2$BF$_4$*Sol*$_{0.5}$ (*Sol* = 1,1,2-Trichloroethane, 1,2-Dibromoethane, 1,2-Dichroloethane)

Akira Miyazaki,* Isao Ichikawa, Toshiaki Enoki,* and Gunzi Saito†

Department of Chemistry, Tokyo Institute of Technology, 2-12-1 Ookayama, Meguro-ku, Tokyo 152

†Department of Chemistry, Kyoto University, Sakyo-ku, Kyoto 606-01

(Received April 7, 1997)

The crystal structures and phase transition nature of (BEDT-TTF)$_2$BF$_4$*Sol*$_{0.5}$ (*Sol* = TCE, DBE, and DCE) are investigated by means of X-ray diffraction, electrical conductivity, ESR, and magnetic susceptibility measurements. As the size of the neutral molecules become smaller (TCE > DBE > DCE), the metal-insulator transition temperature rises (60 K < 100 K < 110 K), showing that their transitions are governed mainly by the structural degrees of freedom. For the DBE and DCE salts, these transitions are simple metal-insulator transitions, whereas the transition of the TCE salt occurs only when the sample is cooled slowly, and the Fermi surfaces survive in the resulting low-temperature phase. For this salt, the anomaly of the interplanar resistivity appears at ca. 160 K for the slow cooling process, and the difference of the ESR line width between the slow and rapid cooling processes is also observed below this temperature. These phenomena are due to the disorder enhanced by the generation of the in-plane superlattice.

It is recognized that many radical ion salts based on the organic donor molecule BEDT-TTF (= bis(ethylenedithio)-tetrathiafulvalene) undergo metal-insulator transitions, some of whose origins are understood as the consequence of the structural change associated with the freeze of the internal degrees of freedom within the molecules. For example, the appearance of the incommensurate superstructure of β-(BEDT-TTF)$_2$I$_3$ at 125 K[1] is understood as a sinusoidal ordering of the conformation of the six-membered dihydrodithiin rings fused to the TTF skeletons of the donor molecules. The rotational motion of the counter anion can also play an important role in the realization of the structural transition. In the crystal of (BEDT-TTF)$_3$(ClO$_4$)$_2$,[2] tetrahedral ClO$_4^-$ anions are rotated around one Cl–O bond at room temperature. This motion is quenched at low temperatures, resulting in the orientational change of the donor molecules, which makes the electronic structure of the salt band insulator below the transition temperature (T_{MI} = 171 K). If this rotational motion is restricted by introducing intermolecular hydrogen bonds between counter anions, namely if the anion is substituted into HSO$_4^-$ anion, this structural phase transition does not appear, and the feature of the strong electron correlation is emphasized in the mechanism of the metal-insulator phase transition.[3]

(BEDT-TTF)$_2$ClO$_4$TCE$_{0.5}$ (TCE = 1,1,2-trichloroethane) is a two-dimensional semimetallic compound. This salt shows metallic behavior down to 25 K, which is consistent with the existence of the Pauli paramagnetic susceptibility (5×10^{-4} emu mol^{-1}).[4] Below 25 K, there is a remarkable cooling rate dependence. When the sample is quenched by rapid cooling (−5 K min^{-1}), the metallic behavior remains down to 1.4 K.[5] On the other hand, if the sample is cooled slowly (−5 K h^{-1}), a sudden increase of the resistivity is observed at 25 K, suggesting the presence of a phase transition.[6] This transition is not a simple metal-insulator transition, since the resistivity becomes almost constant from 10 K down to 0.8 K, and the Pauli paramagnetic contribution remains half as much as that of the rapidly cooled sample.[4] The occurrence of the transition at 25 K is actually governed by the cooling rate in the temperature range of 205—160 K. In this temperature region, there is a remarkable anomaly in the interplanar resistivity, i.e. the resistivity measured along the normal of the conducting plane;[7] the resistivity begins to increase at 160 K with a broad maximum around 140 K, then decreases again as the temperature is lowered. The X-ray diffraction experiment also evidences that the $2a\times b\times 2c$ superstructure grows in this temperature range.[8] These results suggest that the existence of a structural change in the temperature region of 160—140 K plays a crucial role in the emergence of the phase transition at 25 K.

It is conceivable to assume that the structural change comes from the quenching of the following structural degrees of freedom. The non-centrosymmetrical neutral molecules TCE are located on the inversion centers; hence these molecules are orientationally disordered.[9] In addition, each BEDT-TTF molecules has at least one conformationally disordered dihydrodithiin rings, judging from the highly anisotropic thermal ellipsoids of the carbon atoms of the ring. In order to see if these two sorts of disorders work complementary to or independent of the transition, we substituted the neutral molecule TCE for the centrosymmetrical molecule DCE (1,2-dichloroethane), expecting that only the orientational disorder would be extinguished without changing the crystal structure. The resulting salt has the crystal structure

isomorphous to the TCE salt and turns out to show a first-order metal-insulator transition at 182 K without cooling-rate dependence.[7] X-Ray crystallographic analysis of this salt at room temperature shows that besides the disappearance of the orientational disorder of the neutral molecules, the number of disordered six-membered rings is also reduced. This suggests that the disappearance of the disorder may cause the difference in the feature of the transition in these salts. It is therefore indicated that the orientational disorder of the TCE molecules works complementary to the phase transition mechanism of the TCE salt, although the main origin of the transition can be ascribed to the puckering motion quenching of the dihydrodithiin rings of the donors.

For the TCE salt, unfortunately, the enhancement of the interplanar resistivity[7] and the X-ray satellite reflection intensity[8] accompanied with the superstructure growth is little; hence it is anticipated that the resulting structural modulation is too slight to detect. On the other hand, a large structural deformation caused by the metal-insulator transition makes the DCE crystal crush into powder, which also prevents us from any detailed study of the structural change which accompanies the transition. We therefore tried to find other isostructural salts with similar phase transition phenomena to these two ClO_4 salts and more suitable for the structural study of the phase transition phenomena. Along these lines we preliminarily reported the transport properties of (BEDT-TTF)$_2BF_4Sol_{0.5}$ (*Sol* = TCE, DCE, and DBE = 1,2-dibromoethane).[10] When the TCE molecule is included as the neutral molecule, the phase transition occurs at 60 K only when the sample is cooled slowly, while the DCE and DBE salts show the metal-insulator transitions at 100 and 110 K, respectively, without any cooling rate dependence. From these findings, the phase transition nature of these BF_4 salts are similar to those of the corresponding ClO_4 salts. In this paper, the crystal structure for these three salts and the detailed results of electrical conductivity, ESR and static magnetic susceptibility measurements are reported, with the discussion of the structural contribution to the phase transition mechanisms of these BF_4 salts.

Experimental

Samples were prepared by galvanostatic anodic oxidation of BEDT-TTF (12 mg) at room temperature under argon atmosphere, using tetrabutylammonium tetrafluoroborate (25 mg, recrystallized from freshly distilled ethyl acetate) as a supporting electrolyte, and 16 ml of 1,1,2-trichloroethane (TCE), 1,2-dibromoethane (DBE) or 1,2-dichloroethane (DCE) as a solvent. All solvents were treated with concentrated H_2SO_4, washed successively with water, dried with anhydrous Na_2SO_4, then fractionally distilled in prior to use. Oxidation current was limited less than 0.3 μA, in order to avoid the growth of samples without solvent molecules, (BEDT-TTF)$_3$(BE$_4$)$_2$. Black shiny blocks (typical dimension: $1.5\times1.0\times0.3$ mm^3) were harvested after 3—6 weeks.

Crystal structures of (BEDT-TTF)$_2BF_4Sol_{0.5}$ (*Sol* = TCE, DBE, and DCE) were determined by a single crystal X-ray diffraction method. Samples were mounted on Rigaku AFC-7S four-circle diffractometer, and intensity data were collected within the range of $4.5\leq2\theta\leq55°$, and the absorption effect was corrected empirically (ψ-scan method).[11] Structures were solved with direct methods (SHELXS-86),[12] and then refined with full-matrix least-squares method (SHELXL-93).[13] The positions of hydrogen atoms were calculated geometrically and ride on the attached carbon atoms during the refinement. Cell parameters, the number of measured and observed ($|F_o|>4.0\sigma(F_o)$) data, and final R-factors are summarized in Table 1. Full crystallographic data, atomic coordinates, and equivalent isotropic temperature factors for all atoms, anisotropic temperature factors for non-hydrogen atoms, complete bond distances and angles, tables of observed and calculated structure factors are deposited as Document No. 70040 at the Office of the Editor of Bull. Chem. Soc. Jpn.

DC resistivity of the samples was measured down to 4.2 K, both along and perpendicular to the conducting plate (*ac*-plane) using standard four-probe method. Contacts to the sample were made by gold wire (25 μm) with carbon paste. Magnetic susceptibilities for non-oriented single crystals were measured with Quantum-Design MPMS-5 SQUID magnetometer. Polypropylene straws, which were thermally sealed at their centers, were used as sample cells. ESR spectra were measured for a single crystal sample down to liquid helium temperatures, using a JEOL TE-200 spectrometer equipped with an Oxford ESR910 continuous-flow cryostat and an Oxford ITC503 temperature controller. A sample was mounted on a Teflon® rod using silicone grease, and sealed into a sample tube of 5ϕ diameter with 20 Torr of helium as heat exchange gas (1 Torr = 133.322 Pa). The external field was applied parallel to the *c*-axis for each measurement. For the determination of spin–lattice relaxation time (T_1) and spin–spin relaxation time (T_2), DPPH (2,2-diphenyl-1-picrylhydrazyl, recrystallized from benzene, $T_1 = T_2 = 5\times10^{-8}$ s)[14] was used as a standard sample. The energy band structures of the salts at room temperature were calculated based on the tight-binding approximation[15] using the extended Hückel Hamiltonian according to the Wolfsberg–Helmholz approximation.[16] The coefficients for the Slater-type atomic orbitals are summarized in Table 2. The transfer integral t between HOMOs of adjacent molecules is estimated at $t=ES$, where S is the overlap integral between HOMOs, and E is the energy level of the HOMO of BEDT-TTF donor ($\cong -10$ eV).

Results

The three salts are isostructural to each other, regardless of the incorporated neutral molecules, and also to (BEDT-TTF)$_2ClO_4TCE_{0.5}$.[9] Figure 1 shows the unit cell of

Table 1. Crystallographic Data for (BEDT-TTF)$_2BF_4Sol_{0.5}$

Sol	TCE	DBE	DCE
Space group	$P\bar{1}$	$P\bar{1}$	$P\bar{1}$
a/Å	13.005(2)	12.98(2)	12.97(2)
b/Å	18.566(3)	18.279(9)	18.23(2)
c/Å	7.729(1)	7.824(6)	7.811(6)
α/°	79.59(1)	78.22(6)	78.40(9)
β/°	104.33(1)	105.40(4)	106.01(6)
γ/°	110.97(1)	110.29(6)	111.06(7)
V/Å^3	1677(1)	1666(3)	1655(3)
Z	2	2	2
No. of observed reflections ($\|F_o\|>4\sigma(F_o)$)	4823	3897	4094
R	0.053	0.054	0.079
S (Goodness of fit)	1.07	0.99	1.22

Table 2. One-Centered Coulomb Integrals (I) and Slater Exponents (ζ) for the Slater-Type Atomic Orbitals

	S			C		H
	3s	3p	3d	2s	2p	1s
$-I$/eV	20.0	11.0	5.44	21.4	11.4	13.6
ζ	2.122	1.827	1.5	1.625	1.625	1.3

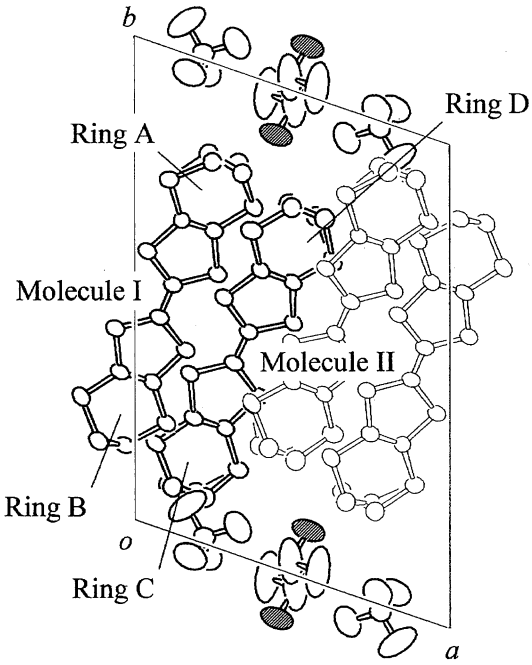

Fig. 1. The unit cell of $(BEDT\text{-}TTF)_2BF_4(TCE)_{0.5}$ viewed along the c-axis. Hydrogen atoms are omitted for clarity. The chlorine atoms indicated with shaded ellipsoids have the site occupancy factors of 0.5, and therefore the TCE molecules are orientationally disordered. Rings A, C, and D are also conformationally disordered.

$(BEDT\text{-}TTF)_2BF_4TCE_{0.5}$ viewed along the c-axis. There are two crystallographically independent BEDT-TTF molecules (molecule I and II), and each molecule has two nonplanar six-membered rings fused to the TTF skeleton (rings A and B for molecule I, C and D for molecule II). The TTF skeleton of the molecule I is planar, while two 1,3-dithiol rings of molecule II are bent from each other by ca. 10°. Besides this, no significant difference in bond lengths and angles are observed between molecules I and II. Among the four crystallographically independent dihydrodithiin rings, rings A, C, and D are conformationally disordered. Table 3 summarizes the site occupancy factors (SOFs) of the major conformers (the conformer which has the larger site occupancy factor) for the dihydrodithiin rings. As the neutral molecule becomes smaller (TCE > DBE > DCE), the SOFs for the ring D become larger (TCE: 0.59(2), DBE: 0.63(2), DCE: 0.70(2)), whereas no distinct tendency is found for the ring C. For ring A, the SOF for the TCE salt is remarkably smaller than the corresponding values for the DBE and DCE salts. For all of these salts, only one conformer is observed for ring B, thus this ring is conformationally ordered. The donor

Table 3. The Site-Occupancy Factors of the Major Conformers of the Four Crystallographically Independent Dihydrodithiin Rings of the BEDT-TTF Donors for the TCE, DBE, and DCE Salts, with the Estimated Standard Deviations in the Parentheses
See Fig. 1 for the locations of rings A, B, C, and D.

	Molecule I		Molecule II	
Sol	Ring A	Ring B	Ring C	Ring D
TCE	0.59(1)	1[a)]	0.51(1)	0.59(2)
DBE	0.81(2)	1[a)]	0.63(1)	0.63(1)
DCE	0.86(2)	1[a)]	0.57(1)	0.70(2)

a) Conformationally ordered.

molecules are aligned with their molecular planes parallel to the *ab*-plane, and the coexistence of the side-by-side (*//a*) and the face-to-face (*//a*+2*c*) intermolecular contacts gives two-dimensional sheets parallel to the *ac*-plane. A number of close S···S contacts shorter than twice of the van der Waals radius of sulfur atom (3.70 Å)[17] are observed in both side-by-side and face-to-face directions. The anion and the neutral molecules are sandwiched between the donor sheets. DBE and DCE molecules have *trans* conformation around the central C–C single bond, which is the most stable conformer for these two molecules. For the non-centrosymmetrical TCE molecule, on the other hand, the chlorine atom at *gauche* position has the occupancy of 0.5 and there is an orientational disorder of the neutral molecule.[18,19]

Figure 2 shows the temperature dependence of the in-plane resistivity for the three salts. All of them are metallic (ρ_{RT} =

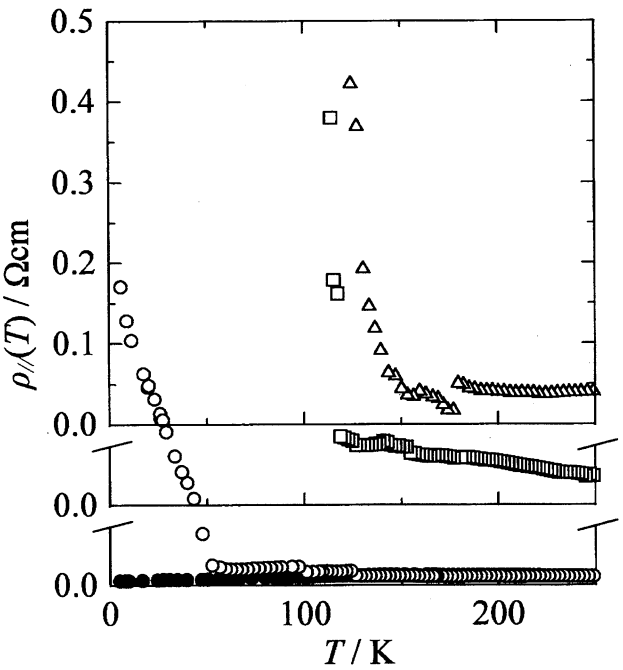

Fig. 2. The in-plane electrical resistivity $\rho_{//}$ of the TCE in the cooling runs under the slow (○: $-5\ K\,h^{-1}$) and rapid (●: $-1\ K\,min^{-1}$) cooling processes. The traces of the DBE (△) and DCE (□) salts in the cooling runs are also presented.

$2\times10^{-2}\Omega$ cm) around room temperature with little temperature dependence in their resistivity. At lower temperatures an abrupt increase of the resistivity is observed, indicating the onset of a phase transition, where the transition temperature (defined as a temperature where $d\rho/dT$ has a maximum) varies by solvent substitution (TCE: 50 K, DBE: 100 K, DCE: 110 K). Below the transition temperature, both DBE and DCE salts show activated-type behaviors within the whole temperature range with the activation energy 1.6×10^3 K for both salts. For the TCE salt, however, the resistivity does not diverge even at the lowest temperature, showing that this transition is not a simple metal-insulator transition, which is similar to the observation for the ClO_4 analogue $(BEDT\text{-}TTF)_2ClO_4(TCE)_{0.5}$.[6] The phase transition behavior for the TCE salt strongly depends on the rate of cooling. If the sample is cooled slowly (-5 K h^{-1}), the transition takes place, while the rapid cooling (-1 K min^{-1}) makes the transition totally suppressed, resulting in the survival of the metallic state even down to liquid helium temperature. For the DCE and DBE salts, the metal-insulator transitions occur regardless of their cooling rates. At the transition point the samples are cracked (DBE salt) or crushed into powder (DCE salt), showing that their metal-insulator transition are first-order in nature, accompanied with a large volume change at the transition point. The interplanar resistivity at room temperature is estimated at $3\times10^2\Omega$ cm for these salts, wihch is 10^4 times larger than in-plane resistivity. Figure 3 presents the temperature dependence of the interplane resistivity of the TCE salt during the cooling process, under the rapid and slow cooling processes. The resistivity shows a broad maximum around 200 K, regardless of the cooling rate. When the sample is cooled slowly (-5 K h^{-1}) a kink of resistivity appears around 160 K accompanied by a subsequent hump, and the transition occurs at ca. 60 K. When the sample is quenched (-1 K min^{-1}), the hump around 160 K does not appear, and the metal-insulator transition at 60 K dose not occur either. This hump in resistivity is not observed for the DBE and DCE salts, regardless of the cooling conditions. The resistivity jump for the slow cooling process which appears in the Fig. 3 and the inversion of the resistivity between the slow and rapid cooling processes around 90 K show no reproducibility, hence they are regarded as artifacts and not intrinsic ones.

Figure 4 shows the temperature dependence of static susceptibility for the TCE and DCE salts after the subtraction of the Pascal core diamagnetism (TCE: -5.15×10^{-4}, DCE: -5.07×10^{-4} emu mol^{-1}). The behavior of the DBE salt is essentially the same as that of the DCE salt. There are Curie spin contributions from defects and/or impurities at low temperatures (concentrations: 1.1—1.6×10^{22} spins mol^{-1}), which are already substracted in the plots in the figure. Around room temperature, the paramagnetic Pauli susceptibilities are observed, whose values (TCE: 6.2×10^{-4}, DCE: 4.1×10^{-4} emu mol^{-1}) are close to the corresponding ClO_4 salts.[4,7] For the DCE salt, the susceptibility is slightly reduced as the temperature decreases above 200 K, below which it decreases gradually and finally approaches exponentially toward zero after the temperature of the metal-insulator transition at 100 K. In the low temperature region below T_c, the paramagnetic susceptibility is expressed as $\chi \propto \exp(-E_A/k_BT)/T$, with the activation energy $E_A = 800$ K. For the TCE salt, on the other hand, the susceptibility is reduced as the temperature decreases and has a minimum value of 5.0×10^{-4} emu mol^{-1} around 70 K. Below this temper-

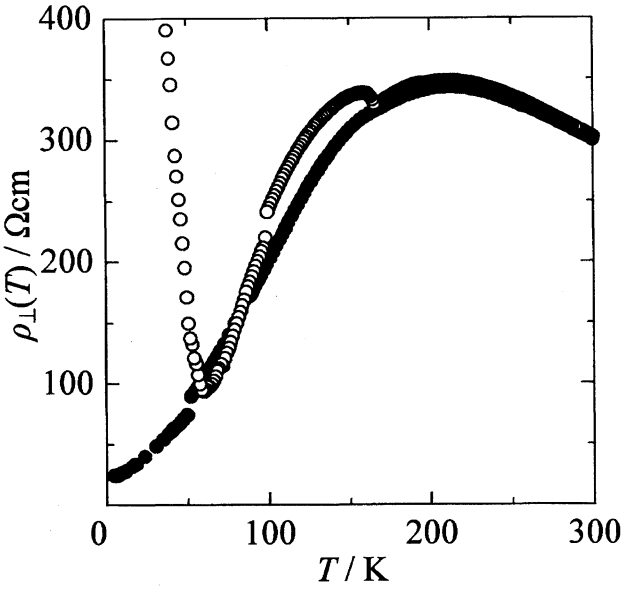

Fig. 3. Temperature dependence of the interplanar electrical resistivity $\rho_\perp$ of the TCE salt in the cooling runs (○: slow cooling, ●: rapid cooling).

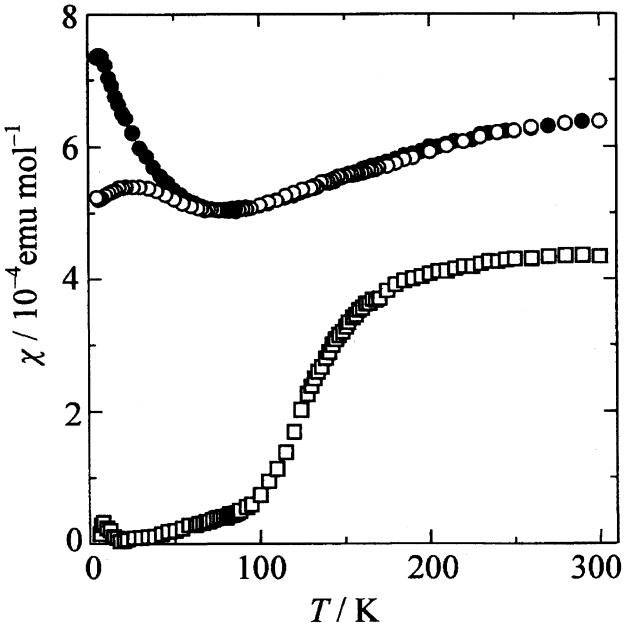

Fig. 4. Temperature dependence of the static magnetic susceptibility of the TCE (○: slow cooling, ●: rapid cooling) and DCE (□) salts, after the subtraction of the contributions of the core diamagnetism and the Curie spins associated with defects and/or impurities.

ature, it increases again to 7.5×10^{-4} emu mol^{-1} at 5 K if the sample is cooled rapidly, whereas under the slow cooling condition only a broad maximum around 30 K is observed, and the susceptibility remains at 5.0×10^{-4} emu mol^{-1} even at 5 K.

On the ESR spectrum, all salts show a single Lorentzian signal of the BEDT-TTF cation radical. The temperature dependence of the ESR intensities for these salts coincides with the static magnetic susceptibilities. Figure 5 shows the temperature dependence of the peak-to-peak line widths for each salt. The saturation measurements give the estimates of the spin-lattice relaxation times (T_1) for TCE, DBE, and DCE salts at 1.8×10^{-7}, 2.4×10^{-7}, and 2.7×10^{-7} s, respectively, at room temperature. From the line widths, on the other hand, the spin–spin relaxation time (T_2) is estimated at 1.3×10^{-9}, 1.4×10^{-9}, and 1.5×10^{-9} s for TCE, DBE, and DCE salts, respectively. Therefore the ESR line widths come mainly from the spin–spin relaxation rate associated with the dipole–dipole interaction and reduced by the motional narrowing. For the DBE and DCE salts, the line widths at room temperature are 2.2 mT and gradually decrease above 160 K with the lowering of the temperature. Below this temperature they begin to decrease more rapidly and then, similarly to the trend of the susceptibilities, they are reduced exponentially with the activation energy 370 and 620 K for DBE and DCE salts, respectively. The line width of the TCE salt (2.7 mT at room temperature) also decreases slowly as the temperature decreases. The temperature where the line width begins to decrease more rapidly depends on the cooling rate, namely, 100 K for the slow (-1 K min^{-1}) cooling and 150 K for the rapid (-5 K h^{-1}) cooling. Below these temperatures the line width decreases not exponentially but linearly with the lowering of the temperature. The cooling rate dependence is observed only for the TCE salt, and for the rest of the salts the traces of the line widths under the rapid and slow cooling conditions coincide within the experimental errors.

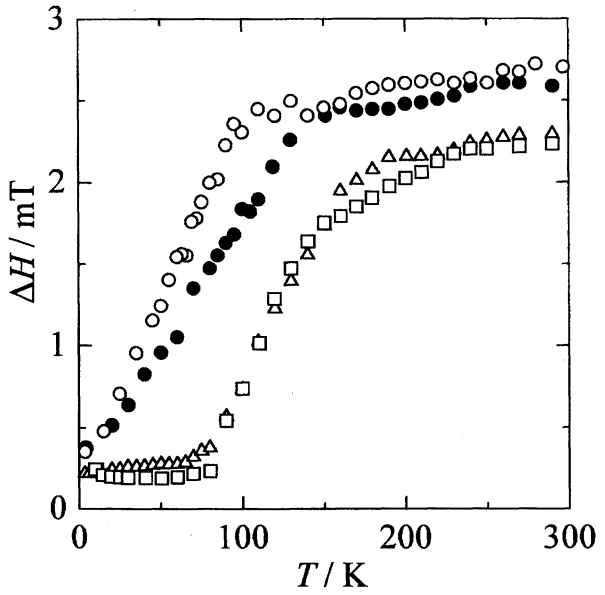

Fig. 5. Temperature dependence of the ESR peak-to-peak line widths of the TCE (○: slow cooling, ●: rapid cooling), DBE (△), and DCE (□) salts, in the external field parallel to the *c*-axis.

Discussion

We first discuss the effect of the solvent substitution on the crystal structure of these salts, by separating the effect into two parts, i.e. the change of the molecular volume and the change of the molecular shape. The molecular volumes of TCE, DBE, and DCE molecules in their most stable conformations are estimated at 86.5, 80.9, and 72.6 Å^3, respectively, by setting the van der Waals radii of C, H, Cl, and Br atoms as 1.70, 1.20, 1.75, and 1.85 Å, respectively,[17] and the C–C, C–H, C–Cl, and C–Br bond lengths as 1.54, 1.06, 1.76, and 1.91 Å, respectively; hence the size of neutral molecules decreases in the order of TCE > DBE > DCE. The change in the molecular volumes of the neutral molecules mainly affects the unit cell volumes of the salts. Comparing the cell parameters of the three salts, the unit cell volume V and one of the cell length b decrease monotonously as the volume of the neutral molecule decreases, whereas the other two cell lengths, a and c, are almost unchanged for the substitution of the neutral molecules. In order words, the presence of the larger neutral molecules makes adjacent two-dimensional donor planes parallel to the *ac*-plane more distant from each other. For the shapes of these molecules, both of the DBE and DCE molecules have C_{2h} symmetry in their most stable conformations, whereas the TCE molecule has an extra *gauche* chlorine atom attached to one of the carbon atoms, and therefore it has C_1 symmetry. The difference in the molecular shape also affects the conformation of the dihydrodithiin rings of the donor molecules. For the TCE salt, three crystallographically independent rings A, C, and D are conformationally disordered. There are no intermolecular contacts shorter than the van der Waals distances around the carbon atoms of rings C, hence rings C can pucker freely. For rings A and D, on the other hand, only one conformer is actually allowed for each site; for the other conformers the intolerably close C···Cl contacts (ring A: 2.82(1), ring D: 3.29(1) Å) are expected to exist between the *gauche* chlorine atom and the carbon atoms of the ethylene bridge group. Hence the conformations of the rings A and D are uniquely determined by the TCE molecule located near these rings, and the disorder of these rings are a consequence of the orientational disorder of the TCE molecules. This situation does not occur for the DBE and DCE salts, since there are no such unendurable carbon–halogen contacts because of the lack of the *gauche* halogen atom. Therefore all of the observed disorders for DBE and DCE salts come from the free puckering motions.

In order to discuss these situations more quantitatively, we define "cavity" as a free space available for the puckering motion of the ethylene groups as follows;[20] At the positions of all the intra- and intermolecular neighboring atoms surrounding an ethylene group, van der Waals spheres are placed, whose radii are set to the van der Waals radii of the corresponding atoms plus 1.2 Å (= van der Waals radius for

hydrogen atom). The cavity is then defined by the closed space surrounded by the concave surfaces of these spheres that encloses the ethylene group. As a typical example, the shape of the cavity for ring C of the TCE salt is presented in Fig. 6, in which the boundary for the cavity is illustrated as a contour drawing in sections separated by 0.05 Å. Table 4 summarizes the cavity volumes of the ethylene bridges belonging to rings A, B, C, and D for the TCE, DBE, and DCE salts. For all of the three salts, the cavity volumes for rings B are remarkably smaller (2.61, 2.23, 2.38 Å^3 for the TCE, DBE, and DCE salts, respectively) than the others, which show that there is little space for puckering around the ethylene groups for these rings. This result agrees with the results of the X-ray analyses, which show that rings B are ordered for all of these salts. On the contrary, the cavities for rings C are especially large (6.45, 5.53, 5.76 Å^3 for the TCE, DBE, and DCE salts, respectively), enough to allow these rings to pucker freely, resulting in the complete conformational disorder of them. We can say from these results that if the cavity volume around the ethylene bridge is large, the six-membered ring puckers more easily. For rings A and D, situations are somewhat complicated. The cavity volumes for these rings for the TCE salt (ring A: 3.18, ring D: 3.65 Å^3) are extraordinary smaller than the corresponding values for the DBE (A: 4.24, D: 4.48 Å^3) and DCE (A: 4.68, D: 4.97 Å^3) salts, although the rings A and D has the site occupancy factors closer to 0.5, i.e. these rings are more disordered than rings A and D of the other salts. This is because the origins of the disorder of rings A and D are actually static ones, as we have mentioned in the previous paragraph. The difference of the cavity volumes between the TCE salt and the DBE, DCE salts is more remarkable for ring A than ring D also from the same reason.

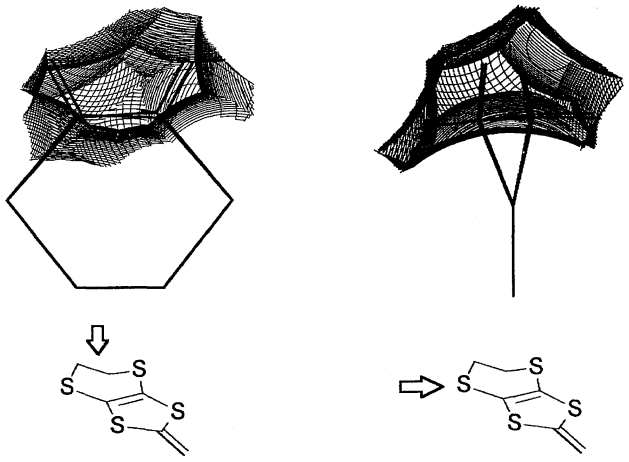

Fig. 6. Cavity for the ethylene-bridge group at ring C of the TCE salt viewed along the directions illustrated below. Thick lines show intramolecular bonds, and thin curves are contours drawing in sections separated by 0.05 Å. See Fig. 1 for the location of ring C.

Table 4. Cavity Volumes (Å^3) for Ethylene-Bridge Groups of the Four Crystallographically Independent Dihydrodithiin Rings (A to D) for the TCE, DBE, and DCE Salts
See Fig. 1 for the locations of rings A, B, C, and D.

Sol	Ring A	Ring B	Ring C	Ring D
TCE	3.18	2.61	6.45	3.65
DBE	4.24	2.23	5.53	4.48
DCE	4.68	2.38	5.76	4.97

Here we compare the electronic structures of these salts, based on the results of the energy band structure calculations. The calculated intermolecular transfer integrals between the HOMOs of the adjacent donor molecules for each salt are listed in Table 5, where the definitions of the overlapping modes between the adjacent donors are presented in Fig. 7. Since the solvent substitution little affects the in-plane cell lengths a and c, the variation of the values of the transfer integrals is generally subtle. Exceptionally, the transfer integrals p_3 and q_3 for the TCE salt are different from those of the other two salts. This can be explained as the result of the steric effect that is caused by the *gauche* chlorine atom of TCE molecule, i.e. this atom pushes the donor molecule aside to change these overlap integrals. However, this steric effect hardly affects the electronic structure of the salts as shown in Fig. 8 for the Fermi surfaces calculated for these three salts. The substitution of the neutral molecule therefore causes little change in the shape of the Fermi surfaces.

The results of the resistivity measurements (Fig. 2) show that all of these three salts undergo phase transitions, whose mechanisms are characterized as structural ones from the following reasons. The transition temperatures are elevated in the order of TCE (50 K) < DBE (100 K) < DCE salt (110 K);

Table 5. Calculated Transfer Integrals at Room Temperature (meV) for $(BEDT\text{-}TTF)_2BF_4Sol_{0.5}$
See Fig. 7 for the definitions of the transfer integrals.

Sol	TCE	DBE	DCE
a_1	83	87	87
a_2	71	78	79
p_1	125	124	125
p_2	171	167	176
p_3	109	126	129
q_1	−44	−45	−44
q_2	−45	−46	−42
q_3	−35	−27	−29

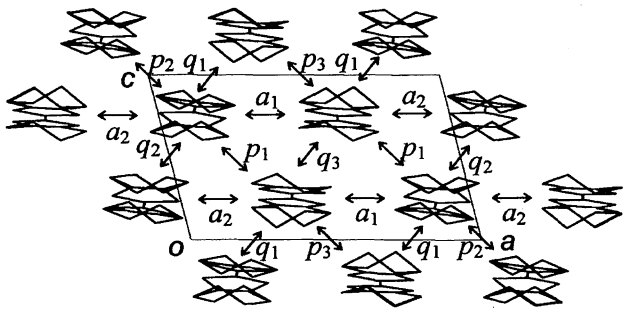

Fig. 7. Schematic drawing of the donor molecule arrangement with symbols for overlap integrals tabulated in Table 5.

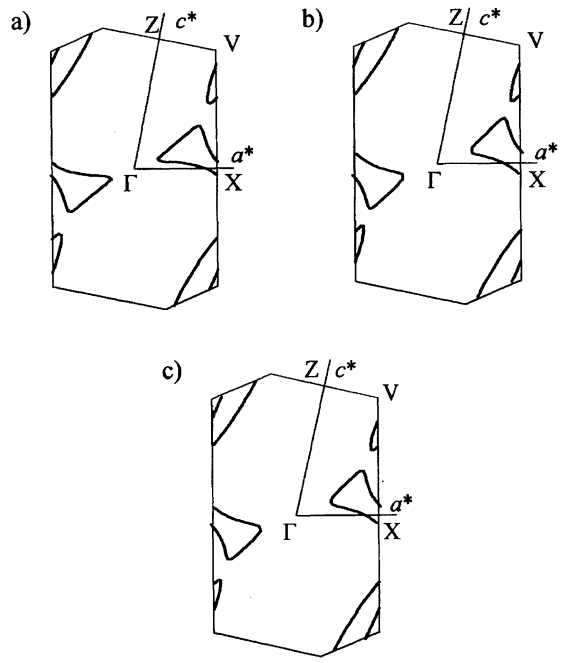

Fig. 8. The Fermi surfaces within the first Brillouin zones for the a) TCE, b) DBE, and c) DCE salts.

especially, there is a large difference between TCE salt and the other two salts. On the other hand, the intermolecular transfer integrals show similar values among these three salts, and the resulting Fermi surface have the similar shapes. If the metal-insulator phase transitions come from the instability of the low-dimensional electronic systems, for example, this mechanism cannot explain the large difference of the transition temperature between the salts with similar electronic structures. More direct evidence of the structural phase transition is the fact that the crystals are cracked at the transition points of the DBE and DCE salts, which shows the large deformation of the crystal structure at their phase transition points.

The origin of the metal-insulator transition of the DBE and DCE salts can be ascribed to the gap opening of the semimetallic band structures, which comes from the structure deformation at the phase transition points. This claim is also supported by the results of the SQUID and ESR measurements; For the DBE and DCE salts, the ESR line width and spin susceptibility show similar temperature dependence, indicating that the line width mainly comes from the spin–spin relaxation and hence depends upon the concentration of the conduction electrons. Therefore it is shown that there is little conduction electron in the low-temperature insulator phase for these two salts. For the TCE salt, on the other hand, the apparent correlation between the ESR line width and the spin susceptibility disappears in the low temperature range. The spin susceptibility of the TCE salt shows no cooling-rate dependence above ca. 60 K and it does not vanish even at liquid helium temperature, regardless of the cooling rate of the sample. This indicates the survival of a metallic state, which gives a finite density of states at the Fermi level under both the rapid and slow cooling processes. On the contrary, the ESR line width of the TCE salt shows the linear temperature dependence and the cooling-rate dependence below 150 K. The increase of the line width below 150 K for the slow cooling process compared to the rapid cooling indicates the increase of the relaxation rate by slow cooling. These results show that the phase transition of the TCE salt at 50 K is by no means only a simple gap opening that occurs at the transition point, as in the case of the other two salts.

We now discuss the reasons for the decrease of interplanar conductivity and the increase of the ESR line width for the TCE salt under the slow cooling processes as shown in Figs. 3 and 5, based on the consideration of the carrier relaxation processes. The interplanar electron conduction is described in terms of the diffusion process in the hopping regime, since the magnitude of the interplanar resistivity is 300 Ω cm. Using the Einstein–Nernst relation the interplanar conductivity $\sigma_\perp$ is expressed as

$$\sigma_\perp = n(E_F) l^2 e^2 / \tau_\perp, \quad (1)$$

where $n(E_F)$ is the density of states at the Fermi level, l is the distance between two conduction planes, and $\tau_\perp$ is the interplanar diffusion time of the conduction electrons. Since there is little difference in in-plane conductivity $\sigma_{//}$ between the rapid and slow cooling processes, we can assume that the quantities $n(E_F)$ and l are independent of the cooling rate. The difference in $\sigma_\perp$ between the rapid and slow cooling processes can therefore be attributed to the difference in $\tau_\perp$. Figure 9 shows the ratio of $\tau_\perp$ between the slow and rapid cooling processes obtained from the interplanar conductivity $\sigma_\perp$. Below 165 K the ratio deviates from unity as the temperature decreases, showing the enhancement of $\tau_\perp$ under the slow cooling process.

The increase of the ESR line width for the slowly cooled sample is ascribed to the same origin. The line width ex-

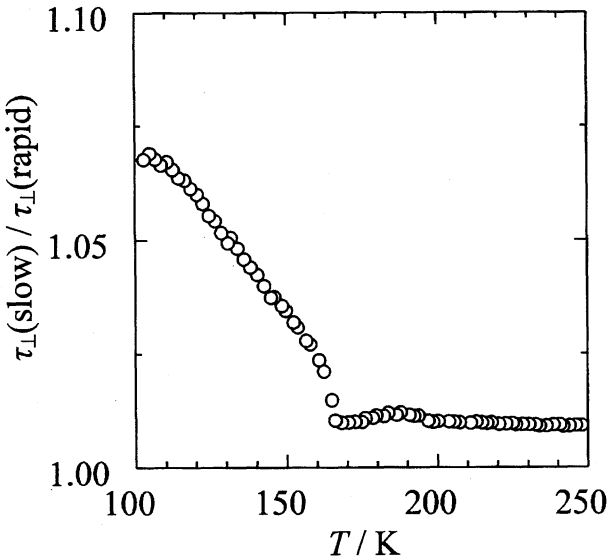

Fig. 9. Temperature dependence of the ratio of the interplanar diffusion time $\tau_\perp$ calculated from the interplanar resistivity $\rho_\perp$, between the slow and rapid cooling processes for the TCE salt.

pected from the dipole–dipole interaction is estimated at 40 mT when the external field is applied along the *c*-axis, on the basis of the second moment calculation assuming that every BEDT-TTF molecule has a half $s=1/2$ spin. Since the observed line width (2.7 mT at room temperature) is ca. 15 times narrower, the effect of motional narrowing due to motion of conduction electron in the crystal is essential. The ESR line width ΔH is then proportional to the product $\langle\omega_d{}^2\rangle\tau_e$, where $\langle\omega_d{}^2\rangle$ is the second moment of the line shape and τ_e is the correlation time for the conduction electron in the crystal. The correlation time τ_e is then expressed in terms of the interplanar diffusion time $\tau_\perp$ and the in-plane relaxation time $\tau_{//}$ as

$$\frac{1}{\tau_e}=\frac{1}{\tau_\perp}+\frac{1}{\tau_{//}}. \tag{2}$$

Because of the absence of appreciable differences in the observed in-plane conductivity between the slow and rapid cooling processes in the temperature range 60 —160 K, the cooling-rate dependence of $\tau_{//}$ is smaller than that of $\tau_\perp$. The correlation time τ_e and the ESR line width ΔH are therefore governed by the interplanar diffusion time $\tau_\perp$.

The origin of the enhancement of $\tau_\perp$ for the slow cooling process is explained qualitatively as follows. The in-plane conductivity $\sigma_{//}$ is written as

$$\sigma_{//}=ne^2\tau_{//}/m^*, \tag{3}$$

where $\tau_{//}$ is the in-plane relaxation time of the conduction electrons, n is the number of the conduction electrons, and m^* is the effective mass. If the condition $E_F\tau_{//}/\hbar\gg1$ holds, two quantities $\tau_\perp$ and $\tau_{//}$ are related by an equation

$$\frac{1}{\tau_\perp}=\frac{t_\perp{}^2}{\hbar^2}\tau_{//}, \tag{4}$$

where $t_\perp$ is the transfer integral between the conducting planes.[21] Recently we found that an $a\times b\times 2c$ superstructure appears after the annealing of the sample at 157 K for 12 h.[22] It is easily assumed that the same superstructure grows in some degree around the same temperature in the present slow cooling process, although the growth of the superstructure is not completed because of the short duration time in temperature region around 157 K. The rate of the in-plane scattering is therefore increased due to the emergence of the disorder during the superstructure generation process, hence $\tau_{//}$ decreases for the slow cooling process. In addition, this disorder also hinders the overlap between the π-orbitals of the adjacent conduction layers, which suppresses the interplanar transfer integral $t_\perp$. These elevate the interplanar diffusion time $\tau_\perp$, which leads to the enhancement of the interplanar resistivity $\rho_\perp$ and the ESR line width ΔH under the slow cooling process.

Finally we compare the results of the BF_4 salts obtained in the present work with those of the corresponding ClO_4 salts. When the neutral alkyl halide molecule is dichloroethane, both the BF_4 and ClO_4 salt undergo the first-order structural phase transition, accompanied with the abrupt disappearance of the conduction electron. Although the collapse of the crystals prevents crystallographical elucidation of the phase transition mechanism, the large transition entropy (40 $J\,K^{-1}\,mol^{-1}=4.8R$) of the ClO_4 salt[7] suggest the importance of the conformational order of the dihydrodithiin rings of BEDT-TTF molecules, whose contribution to the transition entropy is $2.7R$. It is assumed that the same mechanism works also for the BF_4 salt, and the difference of the transition temperature (ClO_4: 182 K, BF_4: 100 K) is presumably due to the size effect of the counter anion. When 1,1,2-trichloroethane is used as a solvent, the resulted salts show at a glance similar behavior regardless of the counter anion. Both salts undergo phase transition only when the samples are cooled slowly in the temperature region around 150 K, where the humps of the interplanar resistivity and growth of the superstructure are observed. The detailed behaviors are, however, different between the ClO_4 and BF_4 salts. The ESR linewidth of the ClO_4 salt shows no significant cooling rate dependency,[23] whereas the BF_4 salt shows larger linewidth below 150 K for the slow cooling process compared to that for the rapid cooling process. In addition, the superstructure vectors which appear around 160 K are also different (ClO_4: $2a\times b\times 2c$,[8] BF_4: $a\times b\times 2c$[22]). The full structural analysis of the superstructure state for the BF_4 salt is now in progress, and the further detailed discussion, such as the reconstruction of the electronic structure, will be presented elsewhere.[22]

Summary

$(BEDT\text{-}TTF)_2BF_4(TCE)_{0.5}$ is a two-dimensional semimetallic molecular conductor, which undergoes a metal–metal phase transition at 50 K only if the sample is cooled slowly ($-1\ K\,min^{-1}$). In order to clarify the mechanism of the phase transition of $(BEDT\text{-}TTF)_2BF_4(TCE)_{0.5}$ in relation to the cooling rate dependence, we investigated isostructural salts prepared by substituting constituent TCE molecules with DCE and DBE molecules having smaller molecular volumes and compared their crystal structures and phase transition nature, by means of X-ray diffraction, electrical conductivity measurement, ESR, and magnetic susceptibility measurement. As the neutral molecule becomes smaller, the unit cell volume decreases, but the band structure calculations reveal that the effect of this cell shrinkage on the electronic structures is relatively small. The solvent substitution modifies the transition from the cooling-rate dependent metal–metal one (TCE salt) to the metal–insulator transitions without cooling-rate dependence (DBE and DCE salts), accompanied by the elevation of transition temperatures (TCE: 50 K, DBE: 100 K, DCE: 110 K). Comparing the rapid and slow cooling processes of the TCE salt, both the interplanar conductivity and the ESR line width are more significantly enhanced in the slowly cooled sample than those of the rapid-cooled one. These results can be understood as the increase of the interplanar diffusion time below 150 K under the slow cooling process due to the disorder enhanced by the incomplete generation of the in-plane superlattice.

References

1) P. C. W. Leung, T. J. Emge, M. A. Beno, H.-H. Wang, J. M. Williams, V. Petricek, and P. Coppens, *J. Am. Chem. Soc.*, **107**, 6184 (1985).

2) T. Enoki, K. Tsujikawa, K. Suzuki, A. Uchida, Y. Ohashi, H. Yamakado, K. Yakushi, and G. Saito, *Phys. Rev., Sect. B*, **B50**, 16287 (1994).

3) A. Miyazaki, T. Enoki, H. Uekusa, Y. Ohashi, and G. Saito, *Phys. Rev., Sect. B*, **B55**, 6847 (1997).

4) M. Kobayashi, T. Enoki, K. Imaeda, H. Inokuchi, and G. Saito, *Phys. Rev., Sect. B*, **B36**, 1457 (1987).

5) G. Saito, T. Enoki, K. Toriumi, and H. Inokuchi, *Solid State Commun.*, **42**, 557 (1982).

6) M. Kobayashi, T. Enoki, K. Imaeda, H. Inokuchi, and G. Saito, *Physica., B*, **143B**, 550 (1986).

7) T. Enoki, Y. Komatsu, K. Suzuki, A. Sekine, Y. Ohashi, and G. Saito, *Synth. Met.*, **70**, 785 (1995).

8) S. Kagoshima, J. P. Pouget, G. Saito, and H. Inokuchi, *Solid State Commun.*, **45**, 1001 (1983).

9) H. Kobayashi, A. Kobayashi, Y. Sasaki, G. Saito, T. Enoki, and H. Inokuchi, *J. Am. Chem. Soc.*, **105**, 297 (1983).

10) T. Enoki, I. Ichikawa, A. Miyazaki, and G. Saito, *Synth. Met.*, **86**, 1971 (1997).

11) A. C. T. North, D. C. Phillips, and F. S. Mathews, *Acta Crystallogr., Sect. A*, **A24**, 351 (1968).

12) G. M. Sheldrick, "SHELXS86, Program for Crystal Structure Determination," Univ. of Göttingen, Federal Republic of Germany (1986).

13) G. M. Sheldrick, "SHELXL93, Program for Refinement of Crystal Structures," Univ. of Göttingen, Federal Republic of Germany (1993).

14) J. P. Goldsborough, M. Mandel, and G. E. Pake, *Phys. Rev. Lett.*, **4**, 13 (1960).

15) T. Mori, A. Kobayashi, Y. Sasaki, H. Kobayashi, G. Saito, and H. Inokuchi, *Bull. Chem. Soc. Jpn.*, **57**, 627 (1984).

16) J. H. Ammeter, H.-B. Bürgi, J. Thibeault, and R. Hoffman, *J. Am. Chem. Soc.*, **100**, 3686 (1978).

17) A. Bondi, *J. Phys. Chem.*, **68**, 441 (1964).

18) In the previous report,[19] non-centrosymmetric space group $P1$ is selected and therefore the alignment of the solvent molecules is fixed to one direction. As no significant change is observed in the Hamilton's test between $P1$ and centrosymmetric $P\bar{1}$ structures we adopt $P\bar{1}$ as the space group and consider the solvated molecules are disordered.

19) B. E. Korotkob and P. L. Sibaeba, *Krystallografia*, **36**, 1454 (1991).

20) Y. Ohashi, K. Yanagi, T. Kurihara, Y. Sasada, and Y. Ohgo, *J. Am. Chem. Soc.*, **103**, 5805 (1981).

21) G. Soda, D. Jérome, M. Weger, J. Alizon, J. Gallice, H. Robert, J. M. Fabre, and L. Giral, *J. Phys. (Paris)*, **38**, 931 (1977).

22) A. Miyazaki, I. Ichikawa, T. Enoki, H. Uekusa, Y. Ohashi, and G. Saito, to be submitted.

23) Y. Komatsu, Master Thesis, Tokyo Institute of Technology.